研 究 解 説　　UDC 532.517.4

A Simple Second-Moment Closure for the Prediction of Turbulent Flows Under the Action of Force Fields
——Part 2 Applications in Flows Affected by Body Forces——
外力が働く乱流場予測に対する簡便な乱れの2次モーメント完結モデルの応用
——その2　体積力の働く流れ場への適用例——

Brian E. Launder*
ブライアン　E.　ロンダー

The paper considers applications of a second-moment turbulence model including force-field influences which has been presented in an earlier communication in this series (Launder, 1989). The applications of the model include shear flows modified by the influence of buoyancy, Coriolis forces and swirl.

1. Introduction

Because second-moment closures handle without approximation the direct effects of force fields on the turbulent stresses, there is the expectation that models of this type should be more successful in predicting such types of flow than ones based on an isotropic eddy diffusivity. In the present contribution the simple second-moment closure presented by Launder (1989) is applied to a range of shear flows that are known to be poorly predicted by the usual k-ε eddy viscosity model.

2. Homogeneous Shear Flow under Stable Stratification (Launder, 1975a)

To begin with, let us consider the behaviour of turbulence in what is nominally a homogeneous horizontal shear flow with a linearly increasing temperature with height. Webster's (1964) measurements of this flow exhibit a great deal of scatter which does not, however, mask the trend of the variations. Later measurements by Young (1975) in a rebuilt version of the same wind-tunnel show very similar behaviour. Figure 1 compares how the relative magnitudes of the normal stresses change as an increasingly stable stratification, expressed in terms of the flux Richardson number R_f ($\equiv -F_{kk}/P_{kk}$) is applied. Note that the stresses are normalized by the turbulence energy so that the three contributions always sum to two. The coefficients c_2 and c_3 in the Isotropization of Production (IP) model** have been taken equal and this choice ensures that the *relative* turbulent kinetic energy in the horizontal direction normal to the mean flow (in this example this direction is denoted x_2 in accordance with usual meteorological practice) is entirely unaffected by buoyancy. This feature, and, indeed, the progressive diminution of the proportion of energy in vertical fluctuations, is well captured by the IP model. The model also predicts a spectacular drop in the vertical: streamwise heat-flux ratio and a progressive rise in the effective turbulent Prandtl

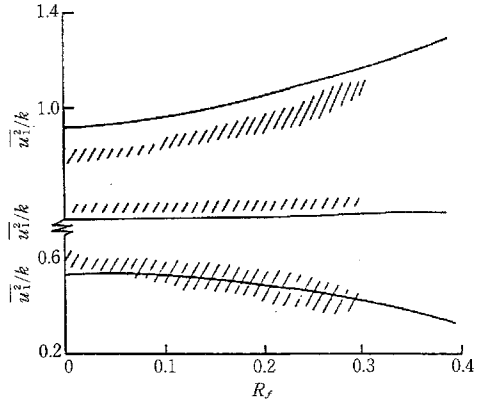

Fig. 1　Relative normal stress levels in nominally equilibrium, homogeneous shear flow under stable stratification ($U_1\{x_3\}$, $\theta\{x_3\}$)
//// band of Webster's (1964) data
—— IP model with $c_2=c_3=0.6$, Launder (1975a)

*Visiting Scientist (UMIST)

**$\varphi_{ij2}=-c_2(P_{ij}-\frac{1}{3}\delta_{ij}P_{kk})$

$\varphi_{ij3}=-c_3(F_{ij}-\frac{1}{3}\delta_{ij}F_{kk})$

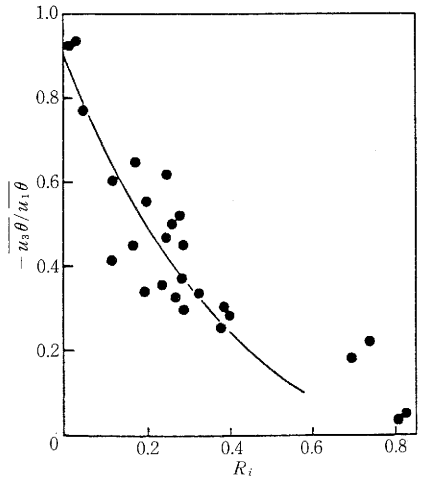

Fig. 2　Ratio of horizontal to vertical heat fluxes in stably stratified homogeneous shear layer, ● ● Webster (1964) experiment; ——IP model, Launder (1975)

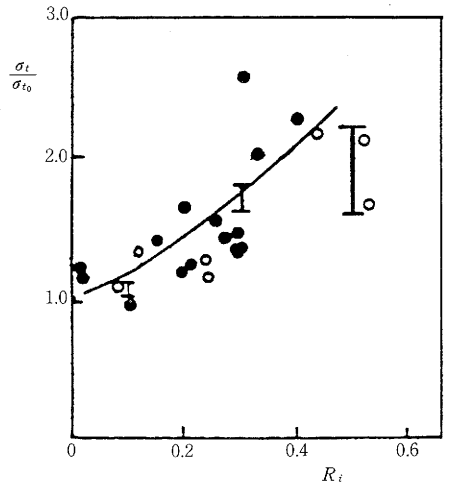

Fig. 3　Dependence of turbulent Prandtl number on strength of stable stratification, ○ ● Experiment, Webster (1964); ——IP model, Launder (1975), II large-eddy simulation, Gerz et al (1988): length of bars indicates range of numerical results (from Gerz et al, (1988))

number, Figures 2 and 3. The latter behaviour is confirmed by very recent large eddy simulations by Gerz et al (1988), the results of which are included in Figure 3.

3. Atmospheric Boundary Layer (Gibson and Launder, 1978)

The inclusion of "wall-reflection" terms***, into the pressure-containing products (as is necessary for handling flows near rigid boundaries) produces a quite different predicted response of the stress field to stable stratification. In this case, Figure 4, the predicted fraction of energy in vertical fluctuations actually *rises* with Richardson number and the experimental data from the lower levels of the atmospheric boundary layer, while scattered, on the whole support this trend. The reason the model produces this paradoxical result is that the stable stratification damps not only the vertical velocity fluctuations but the length scale as well. Thus, the strength of the wall damping (which is proportional to the ratio of the length scale to the distance from the wall) is diminished leading to a relative rise in vertical velocity fluctuations. The varying influence of the wall reflection agency produces complex changes in the ratio of the diffusivities of momentum and heat, K_H/K_M (the reciprocal of the turbulent Prandtl number). Figure 5 shows the atmospheric-boundary-layer data of Businger et al (1971) plotted versus the height normalized by the Monin-Obukhov length scale, L. On this have been superimposed two curves: the direct prediction of the IP model and the model predictions multiplied by 1.2 (the latter on the suspicion, Wyngaard (personal communication), that K_M in the experiments may have been too low by 20% due to

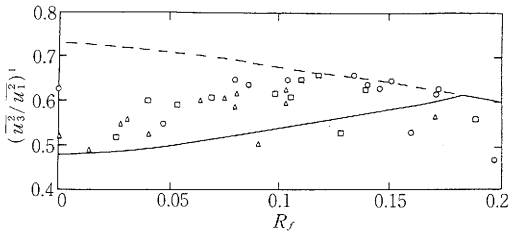

Fig. 4　Dependence on stability of normalized vertical mean square fluctuating velocities in atmospheric boundary layer, ——IP model including wall-reflection terms; ····· IP model without wall-reflection terms, Gibson and Launder (1978); Symbols: expermental data, Businger et al (1971)

***$\varphi_{ij}^{w} = \{c_1'\overline{(u_k u_m}n_k n_m\delta_{ij} - \frac{3}{2}\overline{u_k u_i}n_k n_j$
$-\frac{3}{2}\overline{u_k u_j}n_k n_i)\,\varepsilon/k + c_1'[(\varphi_{km2}+\varphi_{km3})\,n_k n_m\delta_{ij}$
$-\frac{3}{2}(\varphi_{ik2}+\varphi_{ik3})\,n_k n_j$
$-\frac{3}{2}(\varphi_{jk2}+\varphi_{jk3})\,n_k n_i]\}\left[\frac{k^{3/2}}{\varepsilon x_n}\right]^a$

errors in measuring the shear stress). Both curves, but especially the latter, follow the trend of the experiments rather well.

4. Stably Stratified Plane Surface Jet (McGuirk and Papadimitrion, 1988)

An interesting pointer to the importance of wall-reflction terms is provided by the computation of the stably stratified plane surface jet by McGuirk and Papadimitriou (1988). These workers treated the free surface as a symmetry plane except that the same wall-reflection term was added as for near-wall flows. From Figure 6 it is clear that the inclusion of this term greatly improves the predicted temperature profiles across the jet.

5. Rotating Plane Channel (Launder et al, 1987)

Let us now consider the effect of Coriolis forces on the turbulent stress field. Coriolis forces in the momentum equation usually modify the mean velocity field so it is hard to distinguish what part of the change from the corresponding non-rotating flow is associated with the direct action of rotation on the turbulence field itself. However, in a large aspect ratio channel rotating in orthogonal mode, Figure 7, there is no ambiguity for the Coriolis forces in the mean momentum equation are balanced by a variation in static pressure across the channel and no secondary flows are generated. For this reason, unless an *ad hoc* correlation in terms of a rotation parameter is introduced, turbulence models based on an isotropic turbulent viscosity predict that the mean velocity distribution is unaffected by rotation being symmetric about the mid plane and identical to that found in a stationary channel. In fact, even at modest rotation rates the mean velocity distribution, Figure 7b, is far from symmetric. It is easy to see the cause of this asymmetry from the stress transport equation; for the Coriolis terms produce sources of $4\overline{uv}\Omega$ and $-4\overline{uv}\Omega$ in the $\overline{u^2}$ and $\overline{v^2}$ equation (there being no net contribution to the generation of turbulence energy) and a source $-2(\overline{u^2}-\overline{v^2})\Omega$ in the equation for the shear stress $\overline{uv}$. With the chosen coordinates, $\overline{uv}$ is negative near the pressure surface of the channel so the Coriolis terms will act to raise $\overline{v^2}$ and damp $\overline{u^2}$, while (since $\overline{u^2}$ is ordinarily greater than $\overline{v^2}$) its contribution will be to increase the (negative) magnitude of $\overline{uv}$. Near the suction surface the above effects are reversed. Figure 8 compares, for a rotation number, $\Omega D/\overline{U}$, of 0.07, the predicted variations across the channel of v^1 ($\equiv\sqrt{\overline{v^2}}$) obtained by Launder et al (1987) with the large-eddy simulation of Kim (1983); the corresponding profiles for zero rotation are included for comparison. The agreement between the

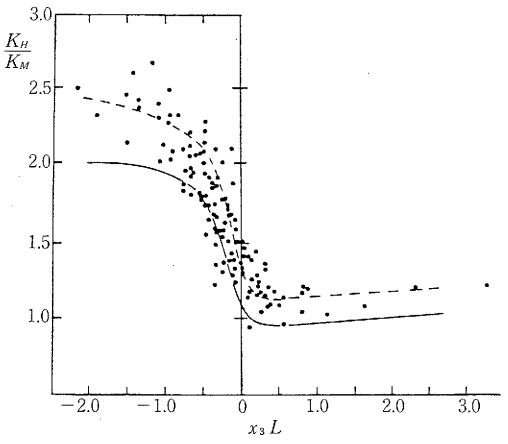

Fig. 5 Dependence on stability of ratio of diffusivity of momentum to heat in atmospheric boundary layer Symbols: experiments of Businger et al (1971), —— IP model including wall reflection, ····· IP model values increased by 20%, Gibson and Launder (1978)

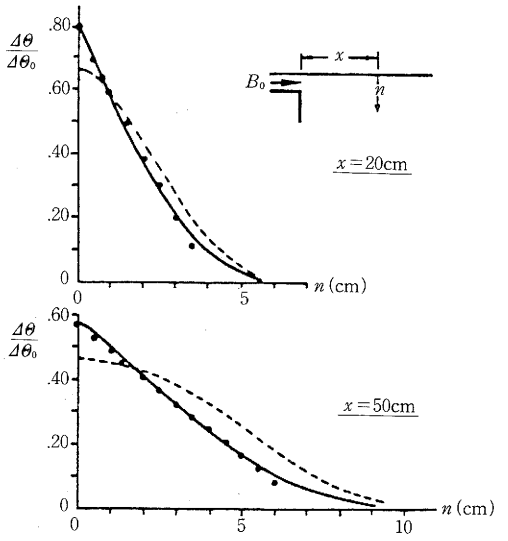

Fig. 6 Temperature profiles in plane free surface jet for initial Froude number of 12, ● experiment; ····· IP model excluding surface-reflection terms; —— IP model including surface-reflection terms (From: McGuirk and Papadimitriou, 1988; reproduced by permission of Oxford University Press)

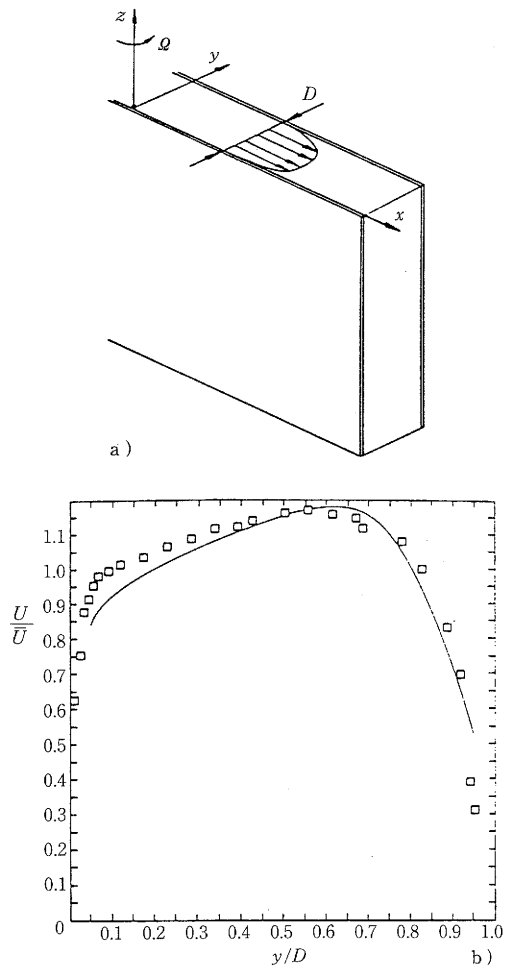

Fig. 7　Mean velocity profile in rotating plane channel, a) configuration and nomenclature b) mean velocity profile for $\Omega D/\bar{U}=0.22$, □ experiment, Johnston et al (1972); ——computation with IP model, Launder et al (1987)

large-eddy simulation and the second-moment computations, while not complete, is broadly satisfactory. From a practical standpoint the effects of rotation of the wall friction are of particular interest. Figure 9 compares the normalized friction velocity on the two walls generated by the second-moment closure with the available experimenatal and computer-generated data. On the suction surface a steady decrease in friction velocity results as the rotation number is raised**** but on the pressure surface, after an initial increase, the friction velocity is essentially uniform for $R_o>0.08$; the computations and experiments agree on this. The reason for this"saturation" is immediately apparent from the Coriolis source. As the rotation number is raised near the pressure surface, $\overline{u^2}$ is progressively depressed while $\overline{v^2}$ is raised. Eventually $\overline{u^2}$ becomes less than $\overline{v^2}$ and at this point the Coriolis contribution to the shear stress equation changes sign and beyond this there is no further rise in wall friction.

6. Rotating Duct Flows (Iacovides and Launder, 1987)

In rotating duct flows of industrial interest, secondary flows will of course be important. The survival of gas turbine blades, for example, depends crucially on the supply of cooling air to their internal cooling passages of roughly circular cross seciton. There is a need to know how the friction factor for these passages is affected by the blade's rotation since (with a fixed pressure drop available) this will indicate how the mass flow rate of cool air will be altered, which in turn affects the potential for cooling the blades. The line in Figure 10 shows a correlation of experimental date of the mean skin friction coefficient by Ito and Nanbu (1971) for a long rotating circular tube and the symbols show a series of computations by Iacovides and Launder (1987) employing an algebraic second-moment closure over most of the flow but with Van Driest's (1956) form of the mixing-length hypothesis used to bridge the semi-viscous sublayer. Excellent agreement between computation and experiment is achieved. However, this is a flow where the Coriolis-induced secondary *mean* velocity field seems to be the dominant factor for computations by the same authors using the k-ε eddy-viscosity model (EVM) also produced very satisfactory accord with the data.

7. Confined Coaxial Jets with Swirl (Hogg and Leschziner, 1988a, 1988b)

The final examples considered are the confined swirling jets measured by Professor So and his team at Arizona State University (So et al, 1984; Ahmed and So 1986) which have been the subject of computations by Hogg and Leschziner (1988a, 1988b). The

****At high rotation rates the experiments of Johnston et al (1972) show a reversion to laminar flow on the suction surface and thus display a precipitate decrease in wall friction. The computations cannot mimic this behaviour as the flow is forced to satisfy turbulent local equilibrium boundary conditions at the edge of the viscosity affected sublayer.

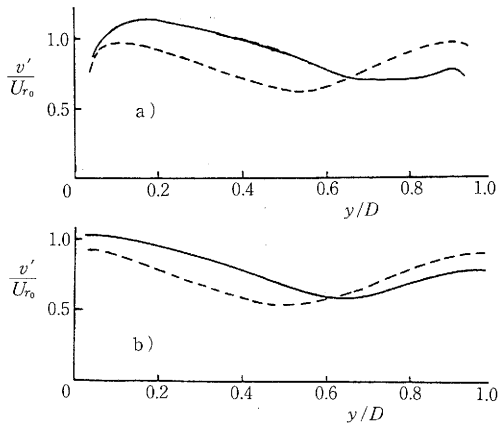

Fig. 8 Variation of rms turbulent velocity normal to plates, a) large-eddy simulation, Kim (1983) b) IP model, Launder et al (1987), ——R_e=24600, R_o=0.07 ; ----- R_e=24600, R_o=0.00

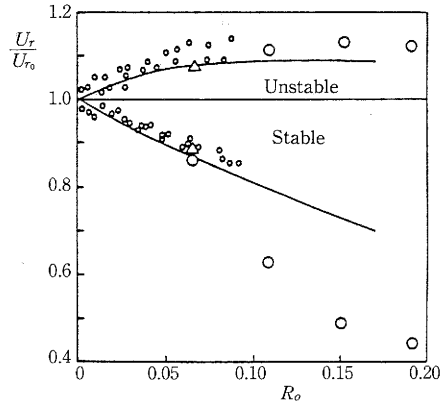

Fig. 9 Variation of normalized velocity on stable and unstable surfaces with rotation Symbols: experimental data obtained and collected by Johnston et al (1972), △ large-eddy simulation, Kim (1983); —— IP model, Launder et al (1987)

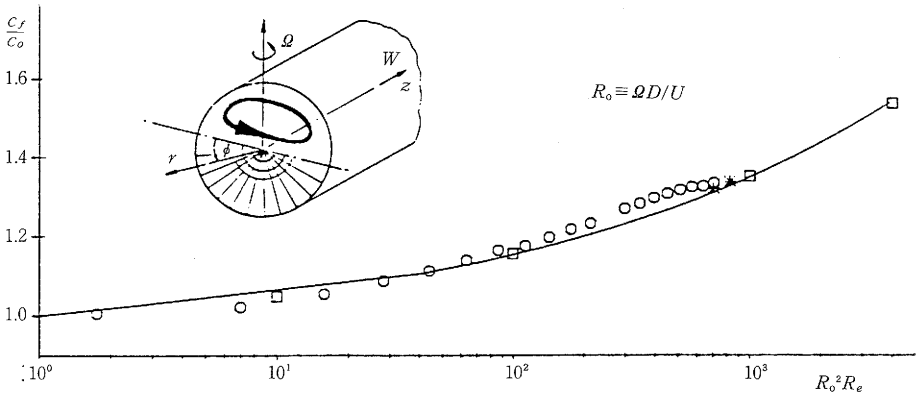

Fig. 10 Normalized friction factor for fully-developed folw in a pipe rotating in orthogonal mode ——correlation of experimental data, Ito and Nanbu (1971)
Symbols: computations, Iacovides and Launder (1987) based on ASM version of IP model

flow arrangement is shown in Figure 11 a pair of confined coaxial jets, the outer one of which is swirling, undergo mixing at a rate enhanced by the thick lip of the inner pipe. In Figure 11 both streams are air at the same temperature. The fact that the core jet is non-swirling at discharge tends to inhibit mixing between the streams and this is why, despite the thick lip to the pipe, the velocity maximum on the pipe axis remains clearly visible ten diameters downstream. Two sets of computational results are shown: those obtained with the standard k-ε eddy-viscosity model and those with the standard IP model presented above. Evidently the latter model succeeds in capturing broadly the measured flow development. With the EVM, however, the velocity peak has disappeared by five diameters downstream, while at x/D=20 all the fluid outside the viscous layer is in solid-body rotation. Broadly similar types of swirling flows have also been studied by Weber et al (1986) with both second-moment and eddy-viscosity models. Their results fully support the conclusions drawn from Figure 11.

Figure 12 considers the case where the inner jet is composed of helium gas. Now the large density difference between the inner and outer streams further impedes mixing; as a result, although the inner jet's momentum is considerably less than for the case considered in Figure 11 the velocity maximum on the axis is still plainly visible twenty diameters down-

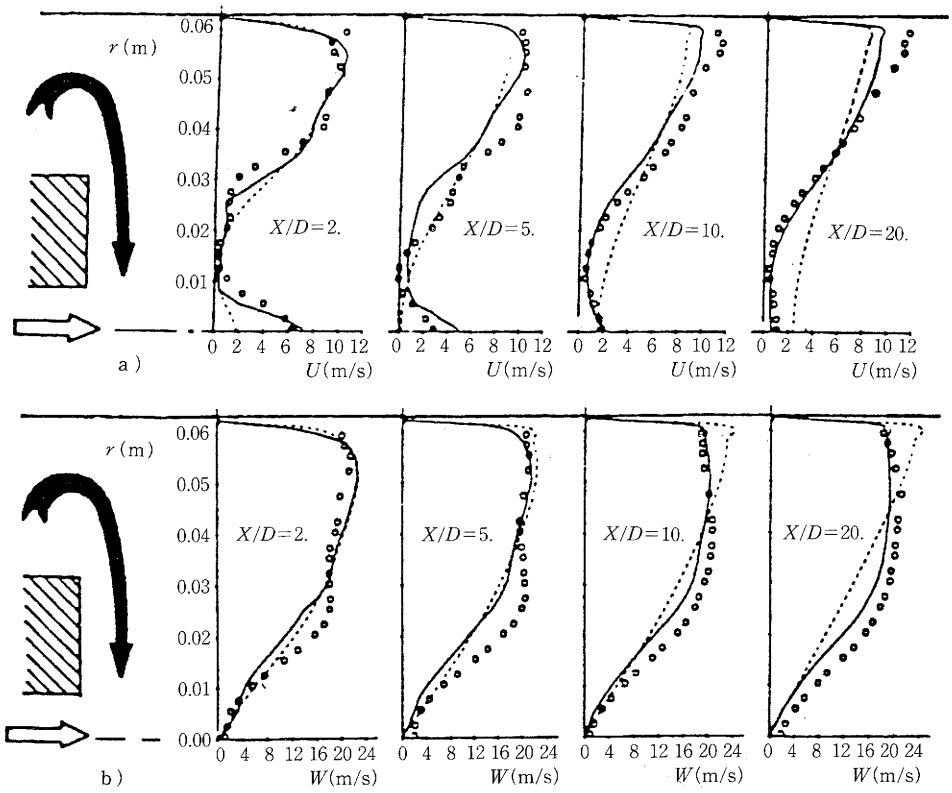

Fig. 11　Development of confined coaxial jets with swirl, ○ ○ experiments, So et al (1984)
——IP model
-----k-ε EVM
} Hogg and Leschziner (1988a), a) axial velocity　b) tangential velocity

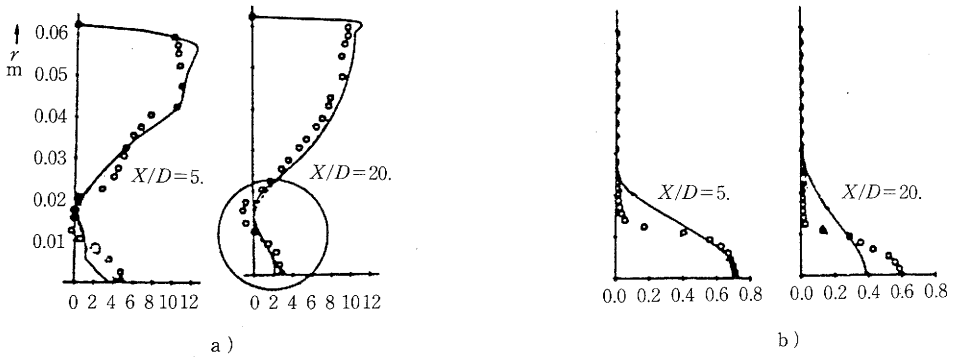

Fig. 12　Development of confined swirling coaxial jets; core jet helium, ○ ○ experiments, Ahmed and So (1986)
——IP model
------ k-ε EVM
} Hogg and Leschziner (1988b), a) axial mean velocity　b) concentration profile

stream. The axial velocity field is very satisfactorily captured by the computation, though we notice from Figure 12 that, even so, rather too much diffusion of the helium has occurred.

8. Concluding Remarks

From the comparisons between computation and experiment provided in the paper it may be inferred that second-moment closures succeed in capturing the effects of force fields on the structure of turbulent

shear flows in a wide variety of circumstances. The inclusion of such models into software for tackling flows of industrial interest is thus very much to be advocated. That recommendation is, however, not to be taken to indicate that no significant further improvements to second-moment closures are likely, still less that none is needed. Several groups in fact are now in the process of developing far more elaborate sub-models for the unknown processes in the second-moment equations designed to comply with various kinematic constraints satisfied by the exact correlation. These schemes have been little tested at present but they hold out the prospect of considerable improvements in predictive capabilities in the near future. The prediction of buoyant flows where density interfaces develop seems especially likely to benefit from these new models. In some flows dominated by force fields it seems that new methodologies may be needed. For example, one usually takes no account of the fact that in the outer region of a free shear flow the fluid at a point is only intermittently turbulent. While in many circumstances this intermittency can be neglected, in a strongly swirling jet discharged into stagnant surroundings "fingers" of jet fluid will tend to be centrifuged radially outward through the non-rotating ambient fluid that surrounds them. It is quite likely that this is why *unconfined* swirling flows are not predicted quite as satisfactorily as the internal flows (Fu, Flaunder and Leschziner, 1987; Fu, 1988). What this suggests is that a good deal more fundamental work is needed to devise ways of incorporating such structural features of inhomogeneous shear flows into second-moment closures.

The paper is based on lectures presented at the Institute of Industrial Science, Tokyo in August 1987 and at the 2nd European Turbulence Conference, Berlin in September 1988. My appreciation goes to all my colleagues in the CFD group at UMIST whose discoveries have been included in this paper. The camera-ready manuscript has been prepared with great care and skill by Mrs. L.J. Ball.

(Manuscript received, November 25, 1988)

9. Nomenclature

a_{ij} dimensionless anisotropic Reynolds stress $(\overline{u_iu_j}-\frac{1}{3}\delta_{ij}\overline{u_ku_k})/k$

A, A_2, A_3 invariants of Reynolds stress field; defined following eq. (20)

$A_{2\theta}$ heat flux invariant $\overline{u_i\theta}\,\overline{u_i\theta}/\overline{\theta^2}k$

$c's$ empirical coefficients

D space between plates or diameter of pipe

f_i fluctuating body force per unit mass

F_{ij} source due to body force in $\overline{u_iu_j}$ transport equation

$F_{i\theta}$ source due to body force in $\overline{u_i\theta}$ transport equation

g_i gravitational acceleration vector

k turbulent kinetic energy

L Monin Obukhov length scale

n_i unit vector normal to wall

P, p mean, fluctuating parts of pressure

P_{ij} generation rate of $\overline{u_iu_j}$ by mean shear

$P_{i\theta_1}$, $P_{i\theta_2}$ generation rate of $\overline{u_i\theta}$ by meantemperature and velocity gradients respectively

R time scale ratio, see eq. (18)

R_f flux Richardson number

R_i gradient Rechardson number

R_o rotation number $\Omega D/\nu$

R_e pipe Reynolds number

U streamwise component of mean velocity

U_i, u_i mean, fluctuating components of velocity in direction x_i

$\overline{u_iu_j}$ Reynolds stress tensor

v' rms velocity fluctuation normal to wall

w tangential component of mean velocity

x streamwise coordinate

x_i Cartesian space coordinate (x_1 denotes stream direction; x_2, x_3 have variable meanings explained in text)

α dimensionless volumetric expansion coefficient

$\Delta\Theta$ excess of temperature above free-stream value

ε dissipation rate of turbulence energy

ε_{ij} dissipation rate of $\overline{u_iu_j}$

ε_θ dissipation rate of $\frac{1}{2}\overline{\theta^2}$

Θ, θ mean, fluctuating parts of temperature

ρ, ρ' mean, fluctuating density

σ_t turbulent Prandtl number

ν kinematic viscosity

φ generalized dependent variable

φ_{ij} pressure-strain correlation

$\varphi_{i\theta}$ pressure/temperature gradient correlation

Ω angular velocity

Ω_k coordinate rotation vector

Subscripts

o value at origin or under neutral or non-rotating conditions

References

Ahmed, S.A. and So, R.M.C. Experiments in Fluids 4, 107 (1986)

Businger, J.A., Wyngaard, J.C., Izumi, Y. and Bradley, E.F. J. Atmos. Sci. 28, 181 (1971)

Chen, C.J. and Rodi, W. "Vertical Turbulent Buoyant Jets: A Review of Experimental Data," HMT Vol. 4, ed. W. Rodi, Pergamon, (1980)

Fu, S. "Computational Modelling of Turbulent Swirling Flows with Second-Moment Closures," PhD Thesis, Faculty of Technology, University of Manchester (1988)

Fu, S., Launder, B.E. and Leschziner, M.A. Paper 17.6, Proc. 6th Turbulent Shear Flows Symp., Toulouse (1987)

Fu, S., Launder, B.E. and Tselepidakis, D.P. "Accommodating the Effects of High Strain Rates in Modelling the Pressure-Strain Correlation," Report TFD/87/5, Mech. Eng. Dept., UMIST, Manchester (1987)

Gerz, T., Schumann, U. and Elghobashi, S.E. "Direct Numerical Simulation of Stratified Homogeneous Turbulent Shear Flows," to appear J. Fluid Mech. (1988)

Gibson, M.M. and Launder, B.E. J. Fluid Mech. 86, 491 (1978)

Hogg, S.I. and Leschziner, M.A. "Computation of Strongly Swirling Confined Flow with a Reynolds Stress Turbulence Model," to appear AIAA J. (1988a)

Hogg, S.I. and Leschziner, M.A. "Second-Moment Closure Calculations of Strongly Swirling Confined Flow with Large Density Gradients," to appear Int. J. Heat and Fluid Flow (1988b)

Iacovides, H. and Launder, B.E. Paper 1-5, Proc. 6th Turbulent Shear Flows Symp., Toulouse (1987)

Ito, H. and Nanbu, K. ASME J. Basic Eng. 93, 383 (1971)

Johnston, J.P., Halleen, R.M. and Lezius, D.K. J. Fluid Mech. 56, 533 (1972)

Kim, J. Paper 6.14, Proc. 4th Turbulent Shear Flows Symp., University of Karlsruhe (1983)

Launder, B.E. J. Fluid Mech. 67, 569 (1975a)

Launder, B.E. "Lecture Series 76: Prediction Methods for Turbulent Flows," Von Karman Institute for Fluid Dynamics, Rhode-St-Genese, Belgium (1975b)

Launder, B.E., Tselepidakis, D.P. and Younis, B.A. J. Fluid Mech. 183, 63 (1987)

McGuirk, J.J. and Papadimitriou, H. Stably Stratified Free Surface Layers with Internal Hydraulic Jumps," in Stably Stratified Flow and Dense Gas Dispersion, ed. J. S. Puttock, Oxford (1988)

So, R.M.C., Ahmed, S.A. and Mongia, H.C. "An Experimental Investigation of Gas Jets in Confined Swirling Air Flow, NASA Report CR-3832 (1984)

Van Driest, E.R. J. Aero. Sci. 23, 1007 (1956)

Weber, R., Boysan, F., Swithenbank, J. and Roberts, P.A. Proc. 21st Symp. (International) on Combustion, 1435-1443, The Combustion Institute (1986)

Webster, C.A.G. J. Fluid Mech. 19, 221 (1964)

Young, S.T.B. "Turbulence Measurements in a Stably Strtified Shear Flow, Report QMC-EP6018, Queen Mary College, London (1975)